Ultrasound in Med. & Biol., Vol. 35, No. 10, pp. 1700–1708, 2009

0301-5629/09/$–see front matter

doi:10.1016/j.ultrasmedbio.2009.04.012

● *Original Contribution*

A NEW 15–50 MHz ARRAY-BASED MICRO-ULTRASOUND SCANNER FOR PRECLINICAL IMAGING

F. Stuart Foster,* James Mehi,† Marc Lukacs,* Desmond Hirson,† Chris White,† Chris Chaggares,† and Andrew Needles†

*Sunnybrook Health Sciences Centre and the University of Toronto, Ontario, Canada; and †VisualSonics Inc., Toronto, Canada

(*Received* 11 *February* 2009, *revised* 6 *April* 2009, *in final form* 19 *April* 2009)

Abstract—Most institutions now have a suite of imaging tools to follow mouse models of human disease. Micro-ultrasound is one of these tools and is second after whole-mouse fluorescence or bioluminescent imaging, in terms of installed systems. We report in this paper the first commercially available array transducer–based ultrasound imaging system that enables micro-ultrasound imaging at center frequencies between 15 and 50 MHz. At the heart of the new scanner is a laser-machined high-frequency 256 element, linear transducer array capable of forming dynamic diffraction limited beams. The power of the linear array approach is embodied in the uniform high resolution maintained over the full field of view. This leads to greatly expanded scope for real-time functional imaging that is demonstrated in this paper. The unprecedented images made with the new imaging system will enable many new applications not previously possible. These include real-time visualization of flow in the mouse placenta, visualization of flow development in the embryo, studies of embryonic to adult cardiac development/disease, and studies of real-time blood flow in mouse models of tumour angiogenesis. (E-mail: Stuart.foster@sunnybrook.ca) Crown Copyright © 2009 Published by Elsevier Inc. on behalf of World Federation for Ultrasound in Medicine & Biology.

Key Words: **High-frequency ultrasound, Micro-ultrasound, Preclinical imaging, High-frequency arrays, Mouse imaging.**

INTRODUCTION

Linear or curvilinear transducer arrays are the dominant technology used in clinical ultrasound imaging. These ubiquitous devices are found in every radiology and cardiology department in the world and are the basis of hundreds of millions of clinical imaging studies each year. The maximum frequencies of clinical systems are typically 12–15 MHz and they can provide resolution on the order of 200 microns at the higher frequencies. In preclinical imaging, where the imaging target is often a mouse, this is a serious limitation because the structures under investigation are often so small that they cannot be resolved. Examples of mouse structures that fall into this category include vessels like the coronary and femoral arteries, the circle of Willis in the brain and the myocardium and other subtle structures of the heart, kidneys and liver. To address this deficiency, scanned single-element transducer systems were developed earlier in this decade (Foster et al. 2002) and now form the basis of most preclinical ultrasound imaging in small-animal models. By preclinical imaging we mean the application of imaging to models of human disease. Several hundred peer-reviewed papers using the single-element scanned micro-ultrasound platform have now been published. In the area of cardiovascular research (Ino et al. 1996; Lee et al. 2008; Liu et al. 2007; Trivedi et al. 2007; Zhou et al 2003, 2004) and in the area of cancer see (Goessling et al. 2007; Kiguchi et al. 2007; Olive and Tuveson 2006; Wirtzfeld et al. 2005, 2006; Xuan et al. 2007). Although single-element systems have fared well in the market, they have serious limitations in depth-of-field and in their ability to provide functional maps of Doppler blood flow in real time. In general, design factors for ultrasound imaging systems are determined by three principle considerations: resolution, maximum imaging depth, and imaging frame rate (Cobbold 2008; Shung 2005). Not surprisingly, these factors cannot be considered independently but must be approached through a

Video Clips cited in this article can be found online at: http://www.umbjournal.org.

The authors are either employed by or have a significant financial interest in VisualSonics.

Address correspondence to: F. Stuart Foster, Rm S-658, Sunnybrook Health Sciences Centre, 2075 Bayview Ave., Toronto, Ontario, Canada M4N3M5. E-mail: Stuart.foster@sunnybrook.ca

series of compromises. For a design in which the dynamic range is expected to be 100 dB, the frequency-dependent attenuation of ultrasound limits the total ultrasound path in tissue to about 600 wavelengths round trip or a maximum depth of 300 wavelengths. Based on this criterion, imaging 10–30 mm of mouse tissue suggests minimum wavelengths of 33 μm (45 MHz) to 100 μm (15 MHz), respectively. Diffraction dictates that resolution in ultrasound is proportional to the product of the wavelength and the f-number (focal length/aperture diameter) of the beam. Thus, an f/2 beam at 45 MHz will have a resolution of approximately 66 μm and at 15 MHz, a resolution of 200 μm. This is ideal for imaging of mice and rats. The new imaging technology reported here enables the frequency of clinical systems based on linear transducer arrays to be extended from 15 MHz to >50 MHz. The transducer technology and high-frequency beamformer at the heart of the system are presented here along with relevant examples of imaging studies of phantoms, normal mouse organs and pathological mouse tissues.

MATERIALS AND METHODS

At the present time no commercially available array transducers are available at frequencies greater than about 15 MHz. For an array transducer to produce a useful beam that can be focused over the desired depth, the aperture should be sampled at $<1.5\lambda$ and preferably less than λ for linear array imaging. The high spatial sampling is needed to prevent unwanted contributions from secondary beams or ''grating'' lobes resulting from undersampling of the active aperture. These requirements are reviewed in Shung (2005). Groups of elements are selected in sequence to transmit and receive ultrasound, building the image one line at a time. The linear array transducer configuration adopted here is to have a total element count of 256, with 64 elements serving as the active aperture at any given time. Scanning of the ultrasound beam is accomplished by multiplexing the groups of 64 elements along the array. There is no limit to the number of lines that can be beamformed, but a trade-off must be struck between frame rate and line density because a beamformed line costs a transmit pulse. The number of lines in the image is typically 256 (standard density) or 512 (high density). The array elements used in beamforming are apodized at the edges of the array but the line density is constant. Given the speed of sound in tissue (1.5 mm/μs), a maximum frame rate of 200 per second can be achieved for a penetration of 15 mm using the standard line density. A 64-channel digital beamformer has been developed. Aspects of the beamformer design are given in Table 1. Essentially quadrature baseband sampling of the radiofrequency signal from each element is performed at a period corresponding to the center frequency of the transducer. A proprietary FPGA architecture is used to clock coarse and fine delays required for dynamic focusing on receive. Up to four transmit focal zones are possible and steering angles of $\pm$ 15° can be achieved for Doppler studies. Table 1 provides additional information on the beamformer implementation. The beamformer and linear array transducers described here were integrated into a completely new high frequency imaging system manufactured by VisualSonics, Toronto. The new scanner is referred to as the Vevo 2100.

Table 1. 64-channel beamformer characteristics

Beamformer design	
Number of transmit channels	64
Number of receive channels	64
Sampling type	Baseband quadrature
Number of bits per channel	10
Transmit delay resolution	1/16 Tx clock period
Receive delay resolution	1/16 Rx sample clock period
Receive fine delay method	Interpolation
Receive focus	Dynamic, updated with every sample
Receive frequency band	4–68 MHz
TGC Gain range	48 dB
System dynamic range (receive)	80 dB

In terms of implementation of high-frequency array devices, the most difficult aspect of the transducer design has been the achievement of the inter-element spacing of approximately one wavelength (30 μm at 50 MHz to 100 μm at 15 MHz). In the age of nanotechnology and submicron very-large-scale integration (VLSI) fabrication, this seems modest; however the active perovskite ferroelectrics such as lead zirconate titanate (PZT) used for transduction have exacting requirements to achieve high efficiency while maintaining sufficient electrical and acoustic isolation from their neighbors to approach the theoretical beamformed performance. These are mostly incompatible with VLSI processes. A number of approaches to achieve high frequency arrays have been demonstrated. Shung (2005) and colleagues (Cannata et al 2006; Ritter et al 2002; Xu et al 2008) and our group (Brown et al. 2007) have reported the use of mechanical dicing approaches to create prototype arrays >20 MHz. Zinc oxide arrays (Weiss et al. 2008) and capacitive micromachined transducers (CMUTs) have also been explored for high-frequency arrays (Johnson et al. 2002; Oralkan et al. 2002). Image quality with such devices has been promising but inconsistent. The approach taken here has been to use eximer laser cutting (λ = 248 nm) to separate and isolate the individual transducer elements in an acoustic stack, as illustrated in the scanning electron micrograph (SEM) of a cross-section through a 30-MHz array structure shown in Fig. 1a. The use of the eximer laser is critical because this ensures a shallow absorption depth and minimizes the heat-affected zone. By optimizing the cutting rate and laser energy it has been possible to create 5–10-μm separations (kerfs) between elements with an

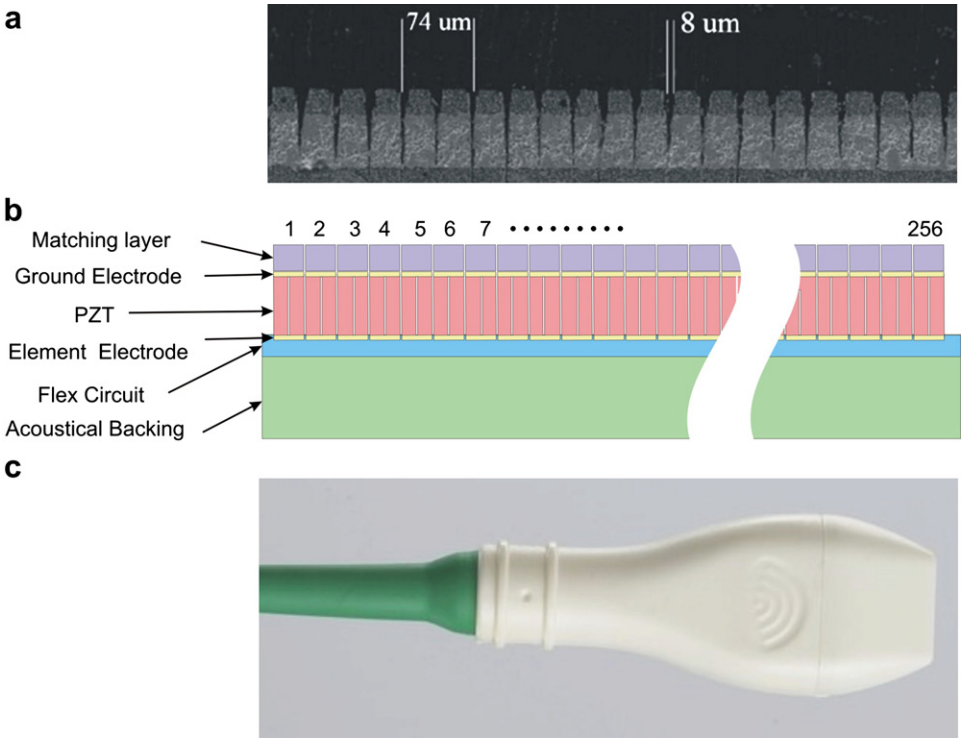

Fig. 1. Construction of a 30-MHz high-frequency linear array. (a) SEM of the active piezo-ceramic (PZT) with laser cuts. (b) Schematic of the acoustic stack showing matching layer, piezo-ceramic, flex circuit and acoustic backing (see Table 2 for layer dimensions). Note that each element is subdiced to reduce lateral resonances. Not shown is an acoustic lens used to focus ultrasound in the elevation direction. A subset of 64 elements is selected from the 256 available elements to form a single line of image information. (c) Assembled 30-MHz probe.

array pitch between 30 and 75 microns without desensitizing (depolarizing) the lead zirconate titanate. Note that each array element is subdiced to minimize lateral modes of oscillation. Thus, the element pitch of this 30-MHz array is 75 μm ($\sim$1.5 λ).

The foundation of a broadband array transducer is based on the careful design of its acoustic stack including a backing, piezoelectric layer (PZT), acoustic matching layers. Our transducer fabrication scheme has previously been reported in detail by Lukacs et al. (2006). A schematic of the high-frequency array architecture is shown schematically in Fig. 1b. In the 15–50-MHz range, the active PZT (3023 HD, CTS Corp.) ranges in thickness from approximately 125 μm to 40μm. For example, the 30-MHz design of Fig. 1a has a PZT thickness of 58 μm. Single or multiple matching layers add an additional thickness of approximately 20 μm per layer to the stack. A concave lens is used to produce an elevation focus at f/4. It was possible to maintain 0.1–1 micron tolerances using the laser fabrication approach. A packaged 30-MHz array is shown in Fig. 1c and its design parameters are given in Table 2 (Transducer 1).

The proof of a successful array implementation is in the quality of the ultrasound beam produced by the device and by the uniformity of transmit and receive beams across the entire array aperture. The array transducer is connected from the flex layer of Fig. 1b to microcoax in the handle of the probe and the 64 channel cable is connected to the beamformer (scanner console) *via* an ITT Cannon connector (DLMB-360P). The transmitted waveform and spectrum for a 30-MHz device (Transducer 1, Table 2) is given in Fig. 2a and 2b, respectively. This waveform was measured with a hydrophone (Onda, HGL-0085, Sunnyvale, CA, USA) positioned at the elevation focus of 9 mm. The pulse has a respectable temporal response and –3-dB bandwidth extending from 20.9–38.5 MHz ($\sim$60%).

Table 2. High-frequency array parameters for devices used in this study

High-frequency array parameters		
	Transducer 1	Transducer 2
Centre frequency (MHz)	30	40
Array length (mm)	15.36	14.08
Element spacing (μm)	60	55
Subdice spacing (μm)	30	27.5
PZT thickness (μm)	45	39
Elevation focal depth (mm)	9	7
Elevation dimension (mm)	2	1.5
Elevation f-number	4.5	4.7

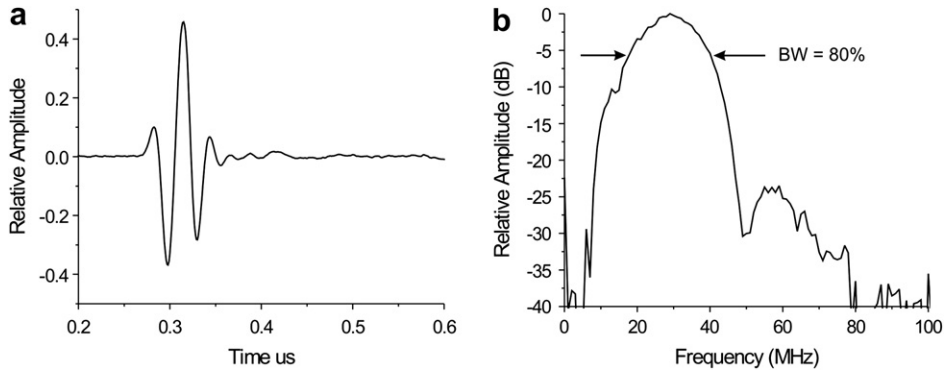

Fig. 2. Measured transmit pulse (a) and spectrum (b) for a 30-MHz array (Transducer 1, Table 1).

The –6-dB bandwidth is 18.7–40.3 MHz. The lateral beam response for Transducer 2 (Table 2) was measured after beamforming by analyzing the pulse echo response from a 25-μm wire at the elevation focus. For the unsteered beam of Fig. 3a, the measured width at half maximum of 103 μm at 30 MHz is somewhat broader than the theoretical value of 92 μm predicted using Field II simulation software (Jensen 2004). This variance is likely because of element-to-element cross-coupling. The grating lobes are below the noise floor for the unsteered beam but steering at 15° resulted in the emergence of grating lobes at approximately the –40 dB level as shown in Fig. 3b and in reasonable agreement with theory.

RESULTS

Phantom studies

Imaging performance with the new digital beamformer and transducer array technology described before was initially evaluated in tissue equivalent phantoms. The phantom material was designed to have attenuation and scattering properties similar to human soft tissue (Ryan and Foster 1997). The geometry of phantoms for greyscale and Doppler imaging are illustrated in Fig. 4. The greyscale phantom (Phantom 1, Fig. 4a) contains 0.5-mm-diameter cylindrical cysts spaced at 2-mm depth intervals, whereas the Doppler flow phantom (Phantom 2) consists of 1.0-mm-diameter flow channels at 2-mm-depth

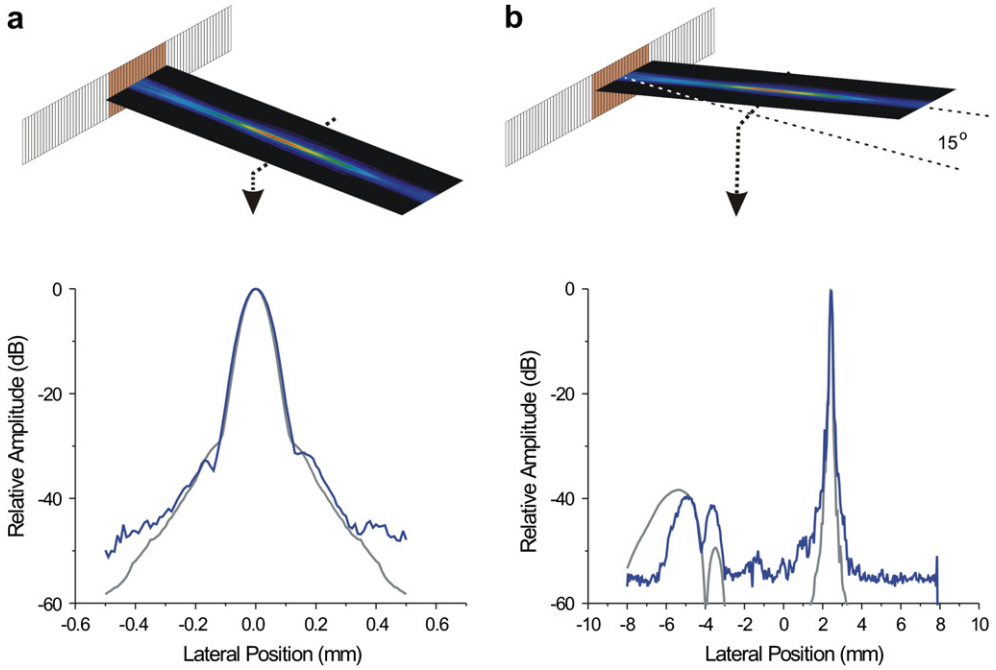

Fig. 3. A subset of 64 elements of Transducer 1 (Table 2) are selected from the 256 available elements to form a single line of image information. Lateral beam profiles for unsteered and 15° steered beams are shown in (a) and (b), respectively. A quantitative comparison of experimental (blue) and theoretical (computed using Field II) beam distributions in the x direction demonstrates good agreement down to less than –40 dB of the on axis amplitude. Some evidence of grating lobes is observed in the steered beam.

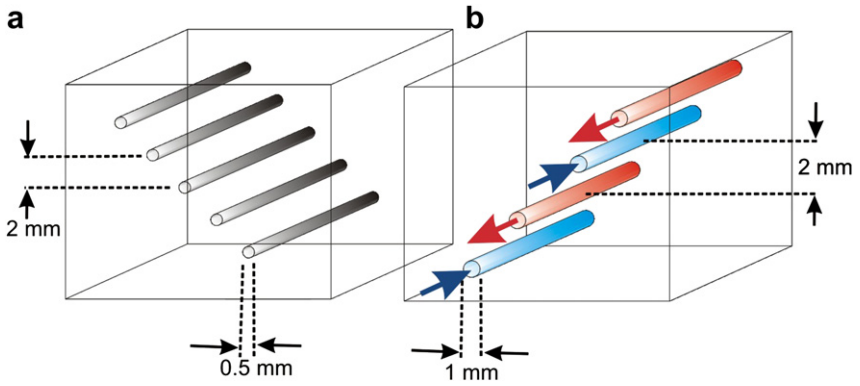

Fig. 4. (a) Gel phantom comprised of cylindrical cystic inclusions 0.5 mm in diameter and spaced at 2-mm depth increments for depth-of-field assessment. (b) Gel phantom for flow imaging comprised of vessel channels 1.0 mm in diameter and spaced at 2-mm depth increments. Flow direction alternates for each channel (*large arrows*).

intervals. Flow direction alternated for each flow channel. Gravity-fed flow of deionized water containing a dilute solution of microbubble contrast (MicroMarker, VisualSonics) was used to generate color and power Doppler images. Images were made using a 40-MHz linear array (Transducer 2, Table 2) and with a 40-MHz fixed focus mechanical probe (VisualSonics Vevo 770). The linear array image of phantom 1 clearly shows 5 targets (arrows) over the entire 10-mm field-of-view (Fig. 5a), whereas the fixed focus transducer only detected 2 targets (Fig. 5b). Similar results are obtained for other fields-of-view at frequencies ranging from 15–50 MHz. Phantom 2 was used to mimic vascular structures to assess Doppler flow mapping capabilities. A long-axis power Doppler image is given in Fig. 5c while pulsed Doppler shows a peak velocity of ~30 cm/s. A short-axis image of phantom 2 is given in Fig. 5e and the corresponding color flow image is given in Fig. 5f. Flow towards the transducer is shown in shades of red and flow away from the transducer is displayed as shades of blue. The parabolic and directional nature of the flow in the phantom is best seen in Fig. 5f.

Mouse imaging

All animal experiments were conducted in accordance with the animal care and use procedures at VisualSonics and conform to the recommendations of the Canadian Council on Animal Care. Cineloops of approximately 800 frames were collected for each experiment at frame rates up to 500 Hz. Mice were anesthetized with 2% isofluorane in oxygen or room air. Body temperature was maintained at 37 °C using a heated, instrumented imaging stage (Vevo Integrated Rail System, VisualSonics). Imaging was performed using a heated gel couplant after local fur removal. Images taken from cardiac studies are given in Fig. 6. Because of the rapid heart rate of the mouse (6–10 Hz) temporal resolution is critical. Frame rates >200 Hz allow good sampling over the cardiac cycle. Figure 6a–6d shows short- and long-axis views of the left ventricle taken from a normal mouse. Figure 6a and 6b shows the contracted heart at end systole, and Figure 6c 6d show the end diastolic configuration. It is possible to generate full 3-D images of the heart at any time in the cardiac cycle using electrocardiogram (ECG) triggering. This is enabled by the use of direct ECG triggering in the hardware of the system such that images are only taken at a predetermined phase of the heart cycle as the transducer is physically translated over the heart using a 3-D actuator (VisualSonics). Such data yields an accurate measure of ventricular volume, cardiac output and ejection fraction in cardiovascular experiments. Figure 6e shows a color Doppler image of blood flow in the aortic arch at the peak of systolic contraction. In a second mouse, a blue jet of flow in diastole reveals aortic regurgitation.

Images of a range of important mouse imaging applications are given in Figure 7. Figure 7a represents a longitudinal cross-section of a day E12 .5 mouse embryo made using a 40-MHz array. The power of the linear array approach is embodied in the uniform high resolution maintained over the full 8 × 8 mm field-of-view showing details of the ventricles of the brain, the heart and other soft tissue structures. Applications in cancer benefit from the extended depth-of-field of the array system compared with the single-element imager, by enabling anterior and posterior regions of tumor growth to be visualized in the same frame. The multilobulated melanoma xenograft of Fig. 7b can be visualized in 3-D in a matter of seconds. Color flow imaging allows many vascular structures to be probed for the first time. Figure 7c shows the circle of Willis in a day E12.5 embryo *in utero*, whereas Fig. 7d shows flow patterns in the placenta of the same embryo. The Doppler images also show flow patterns in large vessels such as the mouse carotid (Fig 7e). Such capabilities are of value in research in the area of atherosclerosis.

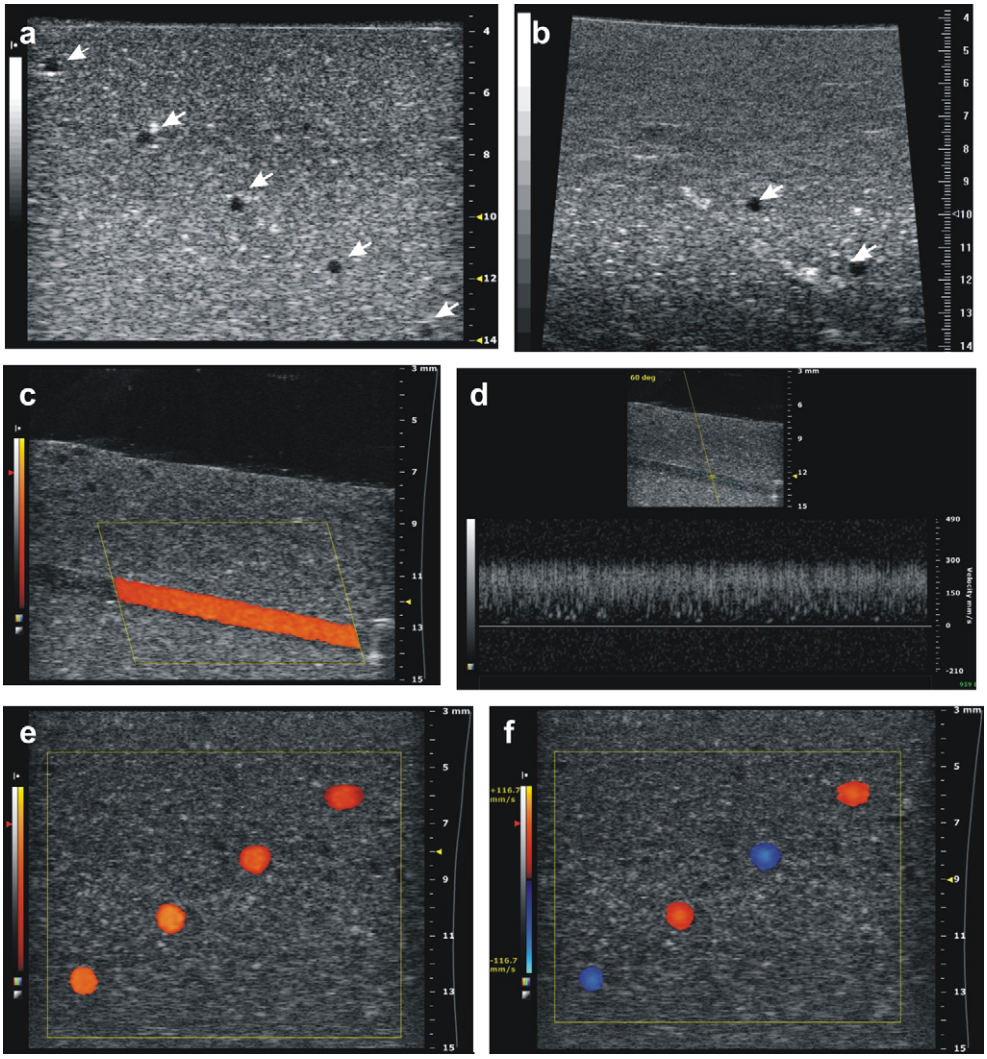

Fig. 5. Images of a tissue equivalent phantom consisting of 500-μm ''cysts'' spaced at 2-mm depth increments: (a) 40 MHz linear array (Transducer 2,Table 1) and (b) 40-MHz single-element transducer. *Arrows* show expanded depth-of-field for the array. (c) Power Doppler of one ''vessel'' of phantom 2 in long axis uses the steering feature to improve the Doppler angle. (d) Pulsed Doppler of the long-axis vessel shows peak velocities of approximately 30 cm/s. (e) Short-axis view of phantom 2 reveals uniform representation of flow with depth and the directional nature of real-time color flow is seen in (f) and in supplementary Video 1. Velocity is encoded such that that shades of red represents flow toward and blue represents flow away from the transducer.

DISCUSSION AND CONCLUSIONS

The frequency of linear array technology for ultrasound imaging has long been mired in the 2–15 MHz range. The array technology reported here extends the bandwidth of high-performance ultrasound imaging from 15–50 MHz, enabling significant improvement in performance for preclinical and potentially clinical applications. The new system is based on a 256-element array configuration with a 64 channel beamformer. Laser machining is used to define the array structure providing kerf widths in the 5–10 μm range. At 40 MHz, the array pitch is 55 μm, with subdicing at 28 μm (Transducer 2, Table 2). The architecture of the transducer and beamformer enable beam profiles that approach the diffraction limit, as shown in Fig. 3. Grating lobes at about –40 dB appear for steering at 15°. Images of phantoms showed dramatic improvement in depth-of-field as seen in Fig. 5a and 5b. One of the major advances associated with the development of the high-frequency micro-ultrasound system reported here is the ability to perform real-time color and power Doppler, as demonstrated in Figs. 5c–5f, 6 and 7. In the preclinical arena, the new technology will find immediate application in a wide range of small-animal biomedical research. The development of high-frequency arrays obviates the need for mechanical actuation and allows maximum frame rates

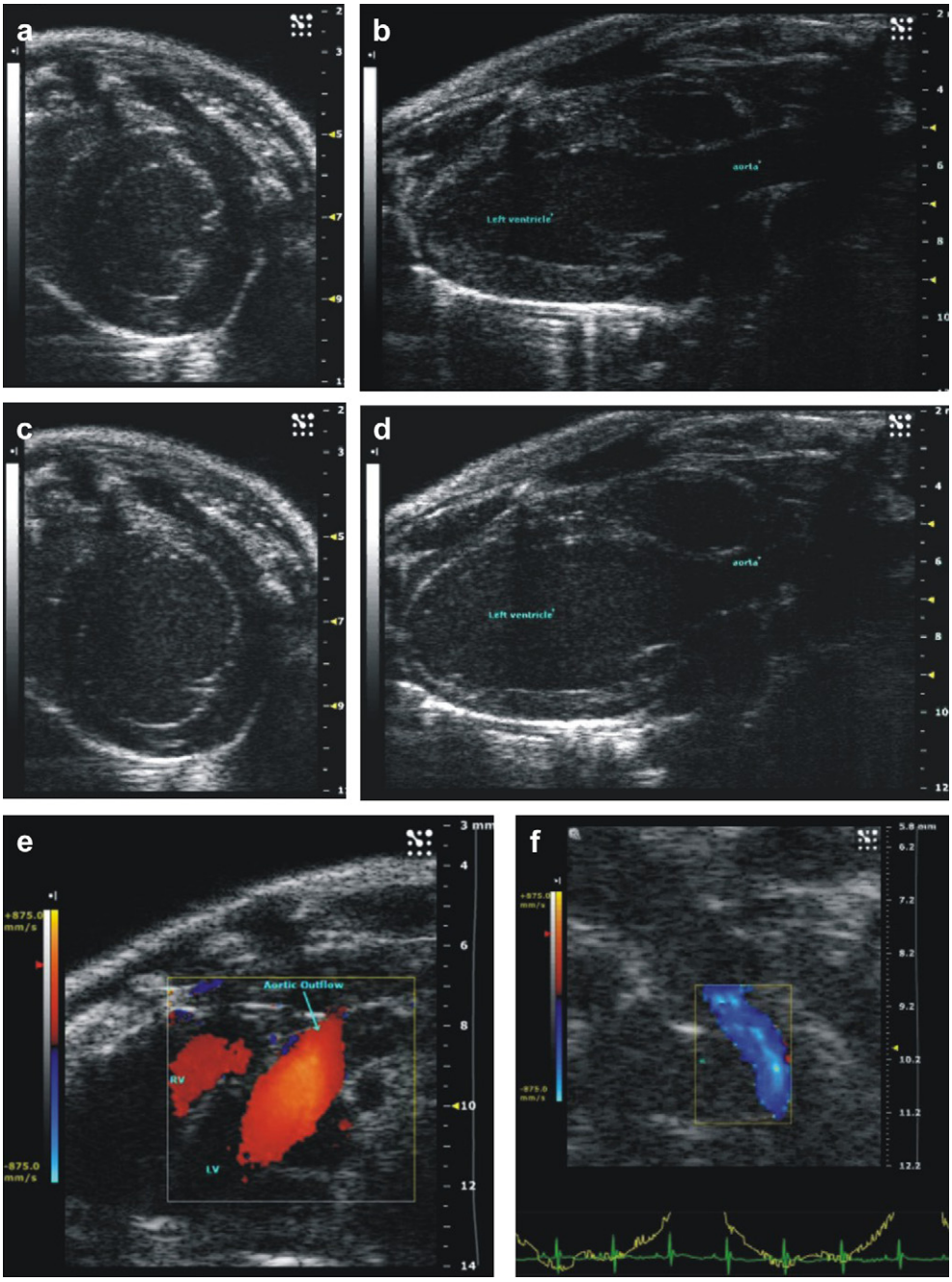

Fig. 6. Images of cardiac structures in the mouse made with Transducer 1 (Table 2). Above short- and long-axis views of the left ventricle at end systole (a, b) and end diastole (c, d). See supplementary Videos 2 and 3 for real-time images of the short- and long-axis views, respectively. Strong forward flow is observed in the aorta with color flow in (d) (supplementary Video 4) and a regurgitant jet is seen in the aortic outflow tract in (e) (supplementary Video 5).

to be limited only by the speed of sound. Previous mechanically actuated systems were limited to frame rates of about 100 Hz. The arrays described here are capable of achieving frame rates of as much as 1000 Hz over limited fields-of-view. For example, one fourth of the lateral field can be imaged at >1000 frames per second, with a 10-mm maximum depth. This is of significant importance to researchers in cardiovascular science, who struggle to understand the biomechanical implications of myocardial infarction or the assessment of novel therapeutics. Equally important are the implications for cancer researchers modeling increasingly complex metastatic models of tumor growth. In addition to providing accurate measures of tumor burden in the parenchymal organs, the array technology enables real-time visualization of flow in the microcirculation using color Doppler and power Doppler.

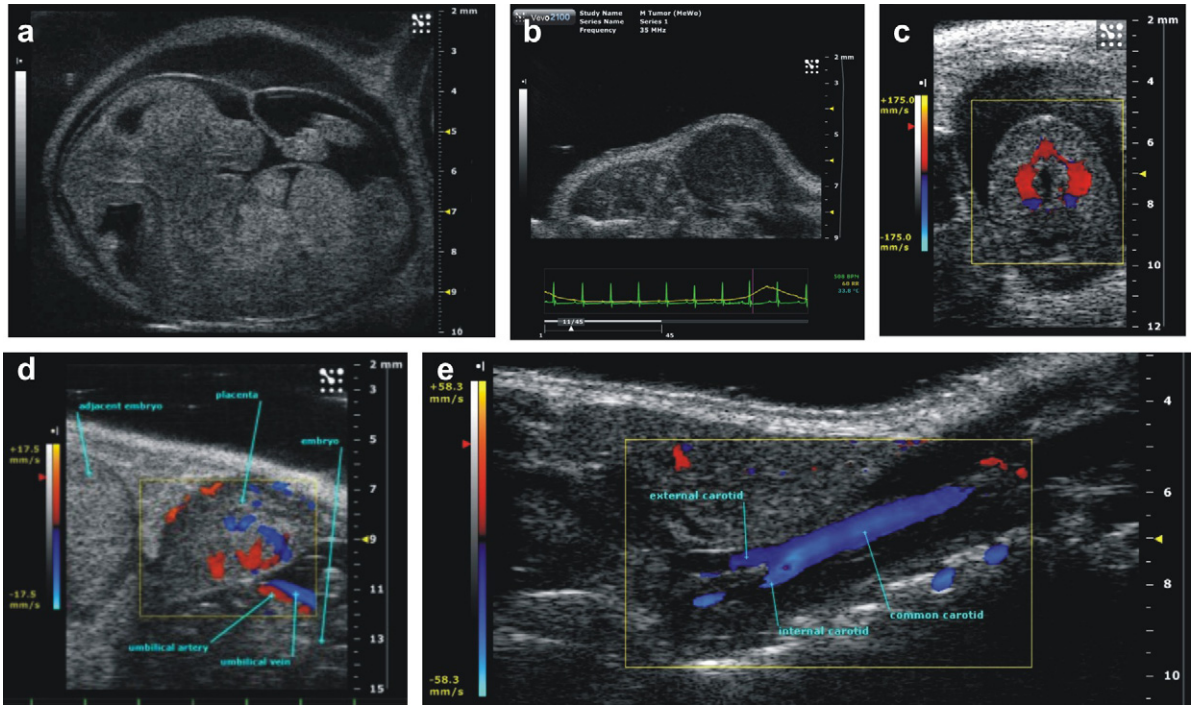

Fig. 7. Images made with the new high-frequency linear array system. (a) Still frame from a real-time image sequence of a day E12 mouse embryo made at 40 MHz (Transducer 2, Table 2) (supplementary Video 5). This long-axis section demonstrates that image resolution is maintained over the full 8-mm field-of-view. Visible are the ventricles of the brain, the developing heart and other structures of the torso. The amniotic sac is clearly visible. (b) 40-MHz image of a human melanoma xenograft showing multilobulated tumor growth. (c) 30-MHz (Transducer 1) color flow of mouse embryonic brain development shows the circle of Willis at day E12.5. (d) 30-MHz image showing the umbilical artery and vein, as well as flow patterns in the placenta. (e) 30-MHz image of a long-axis view of the mouse carotid artery shows the bifurcation into external and internal branches.

Applications in developmental biology, musculoskeletal disease, inflammation, atherosclerosis and a wide variety of other mouse models of human disease will also benefit from the new technology.

SUPPLEMENTARY DATA

Supplementary data associated with this article can be found in the online version, at doi:10.1016/j.ultrasmedbio.2009.04.012

Acknowledgements—The authors gratefully acknowledge the financial contributions of the Terry Fox Foundation, Canadian Cancer Society, Canadian Institutes of Health Research, Ontario Research and Development Fund and VisualSonics.

REFERENCES

Brown JA, Foster FS, Needles A, Cherin E, Lockwood GR. Fabrication and performance of a 40-MHz linear array based on a 1-3 composite with geometric elevation focusing. IEEE Trans Ultrason Ferroelectr Freq Control 2007;54:1888–1894.

Cannata JM, Williams JA, Zhou Q, Ritter TA, Shung KK. Development of a 35-MHz piezo-composite ultrasound array for medical imaging. IEEE Trans Ultrason Ferroelectr Freq Control 2006;53:224–236.

Cobbold R. Foundations of Biomedical Ultrasound. New York: Oxford University Press; 2008.

Foster FS, Zhang MY, Zhou YQ, Liu G, Mehi J, Cherin E, Harasiewicz KA, Starkoski BG, Zan L, Knapik DA, Adamson SL. A new ultrasound instrument for in vivo microimaging of mice. Ultrasound Med Biol 2002;28:1165–1172.

Goessling W, North TE, Zon LI. Ultrasound biomicroscopy permits in vivo characterization of zebrafish liver tumors. Nat Methods 2007;4:551–553.

Ino T, Akimoto K, Ohkubo M, Nishimoto K, Yabuta K, Takaya J, Yamaguchi H. Application of percutaneous transluminal coronary angioplasty to coronary arterial stenosis in Kawasaki disease. Circulation 1996;93:1709–1715.

Jensen JA. Simulation of advanced ultrasound systems using Field II 2004. IEEE International Symposium on Biomedical Engineering 2004;1:636–639.

Johnson J, Oralkan O, Demirci U, Ergun S, Karaman M, Khuri-Yakub P. Medical imaging using capacitive micromachined ultrasonic transducer arrays. Ultrasonics 2002;40:471–476.

Kiguchi K, Ruffino L, Kawamoto T, Franco E, Kurakata S, Fujiwara K, Hanai M, Rumi M, DiGiovanni J. Therapeutic effect of CS-706, a specific cyclooxygenase-2 inhibitor, on gallbladder carcinoma in BK5.ErbB-2 mice. Mol Cancer Ther 2007;6:1709–1717.

Lee DJ, Lyshchik A, Huamani J, Hallahan DE, Fleischer AC. Relationship between retention of a vascular endothelial growth factor receptor 2 (VEGFR2)-targeted ultrasonographic contrast agent and the level of VEGFR2 expression in an in vivo breast cancer model. J Ultrasound Med 2008;27:855–866.

Liu J, Du J, Zhang C, Walker JW, Huang X. Progressive troponin I loss impairs cardiac relaxation and causes heart failure in mice. Am J Physiol Heart Circ Physiol 2007;293:H1273–H1281.

Lukacs M, Yin J, Pang G, Garcia RC, Cherin E, Williams R, Mehi J, Foster FS. Performance and characterization of new micromachined

high-frequency linear arrays. IEEE Trans Ultrason Ferroelectr Freq Control 2006;53:1719–1729.
Olive KP, Tuveson DA. The use of targeted mouse models for preclinical testing of novel cancer therapeutics. Clin Cancer Res 2006;12: 5277–5287.
Oralkan O, Ergun AS, Johnson JA, Karaman M, Demirci U, Kaviani K, Lee TH, Khuri-Yakub BT. Capacitive micromachined ultrasonic transducers: Next-generation arrays for acoustic imaging? IEEE Trans Ultrason Ferroelectr Freq Control 2002;49:1596–1610.
Ritter TA, Shrout TR, Tutwiler R, Shung KK. A 30-MHz piezo-composite ultrasound array for medical imaging applications. IEEE Trans Ultrason Ferroelectr Freq Control 2002;49:217–230.
Ryan LK, Foster FS. Tissue equivalent vessel phantoms for intravascular ultrasound. Ultrasound Med Biol 1997;23:261–273.
Shung K. Diagnostic Ultrasound: Imaging and Blood Flow Measurements. Boca Raton, FL: CRC Press; 2005. 72–73.
Trivedi CM, Luo Y, Yin Z, Zhang M, Zhu W, Wang T, Floss T, Goettlicher M, Noppinger PR, Wurst W, Ferrari VA, Abrams CS, Gruber PJ, Epstein JA. Hdac2 regulates the cardiac hypertrophic response by modulating Gsk3 beta activity. Nat Med 2007;13: 324–331.
Weiss E, Jakob A, Tretbar S, Haberer W, Knoll T, Bauerfeld F, Herrmann J, Lemor R. Micromachined linear array with 100 MHz center frequency. J Acoust Soc Am 2008;123:3784.
Wirtzfeld LA, Graham KC, Groom AC, Macdonald IC, Chambers AF, Fenster A, Lacefield JC. Volume measurement variability in three-dimensional high-frequency ultrasound images of murine liver metastases. Phys Med Biol 2006;51:2367–2381.
Wirtzfeld LA, Wu G, Bygrave M, Yamasaki Y, Sakai H, Moussa M, Izawa JI, Downey DB, Greenberg NM, Fenster A, Xuan JW, Lacefield JC. A new three-dimensional ultrasound microimaging technology for preclinical studies using a transgenic prostate cancer mouse model. Cancer Res 2005;65:6337–6345.
Xu X, Sun L, Cannata JM, Yen JT, Shung KK. High-frequency ultrasound Doppler system for biomedical applications with a 30-MHz linear array. Ultrasound Med Biol 2008;34:638–646.
Xuan JW, Bygrave M, Jiang H, Valiyeva F, Dunmore-Buyze J, Holdsworth DW, Izawa JI, Bauman G, Moussa M, Winter SF, Greenberg NM, Chin JL, Drangova M, Fenster A, Lacefield JC. Functional neoangiogenesis imaging of genetically engineered mouse prostate cancer using three-dimensional power Doppler ultrasound. Cancer Res 2007;67:2830–2839.
Zhou YQ, Foster FS, Nieman BJ, Davidson L, Chen XJ, Henkelman RM. Comprehensive transthoracic cardiac imaging in mice using ultrasound biomicroscopy with anatomical confirmation by magnetic resonance imaging. Physiol Genomics 2004;18:232–244.
Zhou YQ, Foster FS, Parkes R, Adamson SL. Developmental changes in left and right ventricular diastolic filling patterns in mice. Am J Physiol Heart Circ Physiol 2003;285:H1563–1575.

Video Clips cited in this article can be found online at: http://www.umbjournal.org.